Charge-transfer state and state mixing in tetracyanoquinodimethane probed using electroabsorption spectroscopy

ARTICLE

Charge-transfer state and state mixing in tetracyanoquinodimethane probed using electroabsorption spectroscopy

Received 00th January 20xx,
Accepted 00th January 20xx

DOI: 10.1039/x0xx00000x

Ahatashamul Islam,[a] Kensuke Syundo[a] and Toshifumi Iimori *[a]

Tetracyanoquinodimethane (TCNQ) is an important constituent of organic conductors and a versatile electron acceptor. TCNQ exhibited thermally activated delayed fluorescence and an unusually long fluorescence lifetime. In this study, we studied the Stark effect on the absorption spectrum of TCNQ using electroabsorption spectroscopy to gain insights into its photophysics. The electroabsorption spectrum was simulated using multiple absorption bands for different electronic states, which were characterized by different dipole moments and polarizabilities. These electronic states are identified as a locally excited (LE) state with a high oscillator strength and zero dipole moment, and an intramolecular charge transfer (ICT) state with a nonzero dipole moment. The mixing of the LE state with the ICT state is augmented when the molecule is perturbed by an electric field. We provide tangible experimental evidence establishing the key role of mixing between the emissive LE and nonemissive ICT states in the deactivation pathway of electronically excited TCNQ. The dipole moment of the ICT state suggests symmetry breaking of the structure belonging to the D_{2h} point group.

Introduction

The family of 7,7,8,8-tetracyanoquinodimethane (TCNQ) analogues possesses a high electron affinity and has been used to produce molecular assemblies and charge-transfer complexes with donor molecules.[1-3] In the fields of materials chemistry and organic electronics, TCNQ analogues act as versatile electron-acceptor molecules for doping holes into materials. [4-8] Additionally, investigating the excited states of these molecules is important for the development of photoresponsive functional materials based on the TCNQ analogues. [9, 10]

TCNQ is the simplest molecule in the family of TCNQ analogues and can be regarded as an important model system for them. A limited number of studies were reported on the fluorescence spectra of TCNQ more than 30 years ago,[11,12] however, the excited state was not comprehensively studied until recently. Recent studies on photophysics have been performed in the gas phase, solutions, and polymer matrices.[13-19] We previously reported the fluorescence spectra of TCNQ in a variety of solvents. [15] Blue fluorescence of TCNQ was observed in nonpolar solvents, whereas the fluorescence quantum yield (QY) decreased significantly with an increase in solvent polarity. Moreover, an unusually long fluorescence lifetime was observed in hexane and the gas phase. [15, 17] The excited-state dynamics in various solvents were studied using femtosecond transient absorption (TA) and time-resolved fluorescence measurements. [13, 19] The TA dynamics demonstrated that relaxation from an emissive locally excited (LE) state to a nonemissive state occurred within a few picoseconds in polar solvents. [13] Thermally activated delayed fluorescence (TADF) was also observed for carbon tetrachloride. It was hypothesised that the change in the potential energy surface formed by the emissive and nonemissive states led to a change in the fluorescence QY in different solvents and TADF. It was inferred that the nonemissive state was either a triplet or an intramolecular charge transfer (ICT) state. [15, 16] Using laser-induced fluorescence (LIF) spectroscopy, Muramatsu et al. [18] found the fluorescence lifetime to be more than 100 times longer under jet-cooled gas-phase conditions than that in hexane solution. The authors have suggested that the S_1 state is coupled with the higher S_2 state. However, the assignment of the nonemissive state has not been established experimentally to date and remains an open question.

Electroabsorption (EA) and Stark spectroscopies directly provide information about the nature of excited states and their mixing. [20-24] EA spectroscopy, based on the principle of the Stark effect, quantifies the perturbation of the absorption spectra owing to an external electric field by measuring the peak shift and lineshape modifications. [25] It is an optical absorption technique that relies on third-order nonlinear susceptibility and measures only instantaneous changes, thereby mitigating the impact of excited-state interactions with polar environments, such as relaxation after excitation. [21] Moreover, analysis of the EA spectra allows the determination of key molecular parameters, such as changes in the permanent electric dipole moment and polarizability upon excitation. A large dipole moment is associated with the ICT state, which leads to a large

[a] *Department of Sciences and Informatics, Muroran Institute of Technology, Mizumoto-cho 27-1, Muroran, Hokkaido 050-8585, Japan.*
***E-mail**: iimori@mmm.muroran-it.ac.jp*

Electronic Supplementary Information (ESI) available: [parameters of the eight Gaussian bands]. See DOI: 10.1039/x0xx00000x

Stark effect. Therefore, EA spectroscopy is a powerful technique for probing the ICT state [21, 23, 26, 27] and provides valuable insights into the interactions in excited states.

In this study, EA spectroscopy is employed to investigate the photophysics of TCNQ. We show that the absorption spectrum is composed of two electronic states with different dipole moments and polarizabilities. The EA analysis reveals that the nonemissive state has ICT characteristics. It is also reported that the mixing of the emissive and ICT states is augmented in the presence of an electric field perturbation.

Theoretical background of EA spectroscopy

The Stark shift of a transition energy in the presence of an external electric field is expressed as $\Delta E = -\Delta\boldsymbol{\mu}\cdot\boldsymbol{F} - \frac{1}{2}\boldsymbol{F}\cdot\Delta\boldsymbol{\alpha}\cdot\boldsymbol{F}$, where $\Delta\boldsymbol{\mu}$ represents the difference in dipole moment between the excited and ground states ($\Delta\boldsymbol{\mu} = \boldsymbol{\mu}_{\mathrm{e}} - \boldsymbol{\mu}_{\mathrm{g}}$), $\Delta\boldsymbol{\alpha}$ represents the difference in polarizability between these states ($\Delta\boldsymbol{\alpha} = \boldsymbol{\alpha}_{\mathrm{e}} - \boldsymbol{\alpha}_{\mathrm{g}}$), and $\boldsymbol{F}$ denotes the externally applied electric field. Using EA spectroscopy, we measured absorbance changes originating from the Stark shift. The EA spectrum represents the difference spectrum between the absorption spectra recorded in the presence and absence of an external electric field. We can assume that the orientational distribution of the molecules in the ensemble is isotropic for our samples in the absence of an external electric field. For molecular ensembles with an isotropic orientational distribution, the EA spectrum is represented as a superposition of the zeroth, first, and second derivatives of the unperturbed (field-free) spectrum:[20, 24, 25, 28-31]

$$\Delta A(\nu) = (f_{\mathrm{int}}F)^2\left[A_\chi A(\nu) + B_\chi \nu\frac{d}{d\nu}\left\{\frac{A(\nu)}{\nu}\right\} + C_\chi \nu\frac{d^2}{d\nu^2}\left\{\frac{A(\nu)}{\nu}\right\}\right] \quad (1)$$

where f_{int} is the internal field factor; F is the strength of the externally applied electric field ($F = |\boldsymbol{F}|$); χ is the angle between the electric field of light and $\boldsymbol{F}$; ν is the frequency of light; and A_χ, B_χ, and C_χ are the coefficients representing the contributions of the zeroth, first, and second derivatives of the unperturbed absorption spectrum $A(\nu)$ to the EA spectrum, respectively. In this study, TCNQ was dispersed in a rigid polymer matrix; therefore, we assumed that the molecules were immobilized. The coefficients A_χ, B_χ, and C_χ at the magic angle χ = 55° can be expressed as follows:

$$A_\chi = \frac{1}{3|\boldsymbol{m}|^2}\sum_{i,j}A_{ij}^2 + \frac{2}{3\,|\boldsymbol{m}|^2}\sum_{i,j}m_i B_{ijj} \quad (2)$$

$$B_\chi = \frac{\Delta\bar{\alpha}}{2h} + \frac{2}{3|\boldsymbol{m}|^2}\sum_{i,j}m_i A_{ij}\Delta\mu_j \quad (3)$$

$$C_\chi = \frac{(\Delta\mu)^2}{6h^2} \quad (4)$$

where $\Delta\mu$ and $\Delta\bar{\alpha}$ are given by

$$\Delta\mu = |\Delta\boldsymbol{\mu}| \quad (5)$$

$$\Delta\bar{\alpha} = \tfrac{1}{3}\mathrm{Tr}(\Delta\boldsymbol{\alpha}) \quad (6)$$

$\boldsymbol{m}$ is the transition dipole moment in the absence of $\boldsymbol{F}$; and $\boldsymbol{A}$ and $\boldsymbol{B}$ represent the tensors of the transition polarizability and transition hyperpolarizability, respectively. The $\boldsymbol{A}$ and $\boldsymbol{B}$ describe the effect of external electric fields on the transition dipole moment:

$$\boldsymbol{m}(\boldsymbol{F}) = \boldsymbol{m} + \boldsymbol{A}\cdot\boldsymbol{F} + \boldsymbol{F}\cdot\boldsymbol{B}\cdot\boldsymbol{F} \quad (7)$$

where $\boldsymbol{m}(\boldsymbol{F})$ is the transition dipole moment in the presence of an external field $\boldsymbol{F}$; indices *i* and *j* represent the molecule-fixed axes and are used to describe the individual components of the vectors and tensors, respectively; and h is the Planck's constant. The internal field factor, f_{int}, represents a factor that converts an externally applied electric field to a local electric field acting on the molecules in dielectric materials. f_{int} is required to determine the values of $\Delta\mu$ and $\Delta\bar{\alpha}$ from the EA spectrum. However, the estimation of f_{int} for condensed-phase systems is known as a challenging problem in Stark spectroscopy, [20] and thus only the uncorrected values for both $\Delta\mu$ and $\Delta\bar{\alpha}$ are reported. A value of f_{int} is usually assumed to be in the range of 1.1–1.3 for frozen solvent matrices. [20] When a redshift or blueshift of the absorption band is induced by the Stark effect, a first-derivative component appears in the corresponding EA spectrum. A field-induced broadening of the band shape results in the second-derivative contribution, which arises from the change in dipole moment $\Delta\mu$.

Experimental methods

TCNQ (Tokyo Chemical Industry) was recrystallized from acetonitrile and washed with benzene. Polymethyl methacrylate (PMMA; Aldrich, M_W = 120 000) was purified *via* precipitation using benzene and methanol. TCNQ (0.9 mg) and PMMA (0.75 g) were mixed with 3 mL of 1,1,2-trichloroethane (Kanto Chemical, spectroscopy grade) until complete dissolution. A spin-coating technique was used to prepare thin films of PMMA dispersing TCNQ (TCNQ/PMMA). The TCNQ/PMMA solution (1 mL) was spin-coated at 300 rpm for 5 min onto a quartz substrate that was partially coated with a conductive indium tin oxide (ITO) layer (quartz/ITO). Vacuum vapor deposition was used to prepare a semitransparent aluminium (Al) layer on the TCNQ/PMMA film.

EA spectra were measured using the samples with a quartz/ITO/(TCNQ/PMMA)/Al layered structure. The ITO and Al layers were used as electrodes to apply the voltage. The thicknesses of the TCNQ/PMMA films were calculated from the interference fringes in the transmission spectra in the near-infrared region. The typical film thickness was 8.5 μm.

A home-built electric field modulation spectroscopy system was used to obtain the EA spectra. [24] The light beam from the xenon lamp was monochromated, linearly polarized using a polarizer, and directed through the sample substrate to a photomultiplier tube (PMT). A sinusoidal alternating current (AC) voltage with a frequency of $f_0 = 333$ Hz was applied to the sample. The field-induced change in transmitted light intensity $\Delta I(2f_0)$ was detected at the second harmonic $(2f_0)$ frequency of the applied voltage using a lock-in amplifier (LI5640, NF Corporation). A voltmeter was used to record the direct-current (DC) voltage component of the transmitted light (*I*). The EA

spectrum (ΔA) was calculated from $\Delta I(2f_0)$ and I using the following equation:

$$\Delta A = -(2\sqrt{2}/\ln 10)\Delta I(2f_0)/I \quad (8)$$

F was determined by dividing the magnitude of the voltage by the thickness of the TCNQ/PMMA layer. χ was calculated according to Snell's law of refraction, using the reported refractive index for PMMA (n = 1.51).[32] EA spectra were recorded at χ = 55°. For the compensation of the optical path length change across the film with the change in χ, 1/sinχ was multiplied with the absorbance in fitting the EA spectra.[33]

The derivative line shapes of the absorption spectra were calculated numerically. Fitting of the EA and absorption spectra was performed using the curve-fitting function of the IGOR program (WaveMetrics).

Results and discussion

The absorption spectrum of TCNQ in PMMA is shown in Fig. 1a. The absorption maximum is located at 403 nm (2.49 × 10^4 cm^{-1}). This spectrum is consistent with our previous results for PMMA films with the same composition.[14] The EA spectrum acquired at χ = 55° and an electric field strength of 0.3 MV cm^{-1} is presented in Fig. 1c. The EA spectrum exhibits a positive peak at wavenumbers lower than the absorption maximum. A linear relationship is observed between the change in the absorption spectra (ΔA) and the square of the electric field strength, $|F|^2$ (Fig. 2). It is evident from linearity that the spectrum arises from the second-order Stark effect, and eqn. (1) can be used to analyse the spectrum.

If the absorption band in Fig. 1a originates from the transition to a single electronic state, the EA spectrum can be fitted using a single set of coefficients A_χ, B_χ, and C_χ along with the zeroth, first, and second derivatives of the entire absorption spectrum. We attempted to fit the EA spectrum using a single set of coefficients and the entire absorption spectrum (Fig. S1 in the Electronic Supplementary Information). While the fitting was relatively good at wavenumbers above 2.5×10^4 cm^{-1}, the main feature of the EA spectrum observed at 2.3×10^4 cm^{-1} was not fitted properly. This indicates the overlapping of multiple transitions, which have different molecular parameters $\Delta\mu$ and $\Delta\bar{\alpha}$.[23 25]

The excited states of TCNQ were studied using second-order approximate coupled-cluster singles and doubles (CC2) calculations.[35] In this work, the two excited states were predicted within the measured energy range from 2.0×10^4 to 3.2×10^4 cm^{-1}. Further, time-dependent density functional theory (TD-DFT) calculations also predicted two excited states.[17,18] Therefore, it is reasonable to assume two individual absorption bands.

To separate the different transitions, the absorption spectrum was decomposed into a sum of Gaussian bands, thereby allowing the separation of absorption bands with different molecular parameters required for the EA analysis. The preliminary analysis in Fig. S1(a) indicates that the EA spectrum at wavenumbers higher than 2.5×10^4 cm^{-1} mainly arises from the principal component in the absorption spectrum. Moreover, a minor component at lower wavenumbers in the absorption

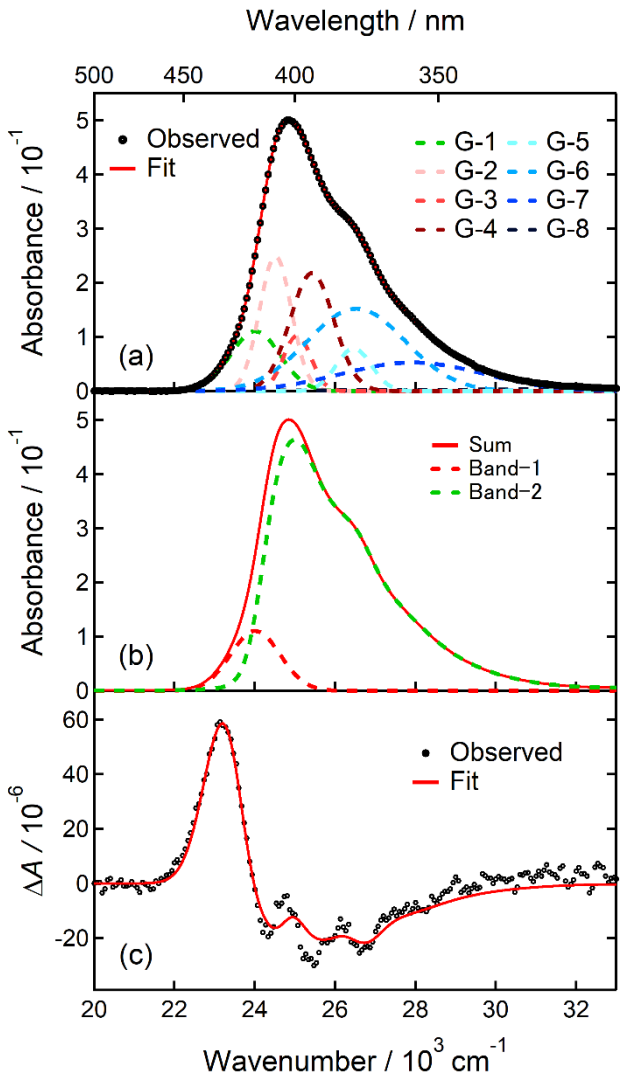

Fig. 1. (a) Absorption spectrum of TCNQ (black circle) in PMMA. The fitting results of the absorption spectrum (red line) with a sum of Gaussian bands (broken lines) are also indicated. (b) Band-1 and band-2 (broken lines) are used to fit the EA spectrum. The sum of band-1 and -2 is indicated by the solid red line. (c) EA spectrum (black circle) obtained at χ = 55° and the fitting result (red line).

spectrum contributes to the main irreproducible EA features. The irreproducible EA component is separated by subtracting the EA spectrum, which is obtained by fitting at wavenumbers higher than 2.5×10^4 cm^{-1}, from the observed EA spectrum (Fig. S1(b)). The extracted EA spectrum possesses the feature of a second-derivative component of the absorption band which has centre energy at approximately 2.4×10^4 cm^{-1}. Therefore, the Gaussian band with this centre energy was used as an initial estimate for fitting the absorption spectrum.

The analysis reveals that eight individual Gaussian bands are required to fit the absorption spectrum, labelled G-1 to G-8, in increasing order of their centre energies (Fig. 1a). Their amplitudes, widths, and centre energies are listed in Table S1 in

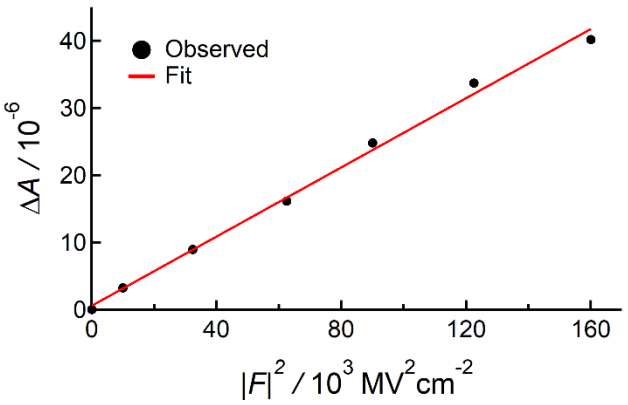

Fig. 2. ΔA as a function of $|F|^2$, and the line fitted to the data (red line). ΔA was monitored at 431 nm.

the ESI. It is reasonable to consolidate Gaussian bands G-1 to G-8 into two groups, each corresponding to two distinct electronic states. The Gaussian band G-1 has a centre energy of 2.40×10^4 cm^{-1}. This Gaussian band is identified as the electronic state which exhibits the second derivative component in the extracted spectrum of the preliminary EA analysis. The second derivative EA spectrum indicates that $\Delta\mu$ is significant upon the transition to this electronic state.

A well-resolved vibrational progression in the transition was studied using the high-resolution LIF spectroscopy in the gas phase.[17,18] The origin band was observed at 24262 cm^{-1}. This energy is in good agreement with the centre energy of the Gaussian band G-2 in the PMMA matrix. The Gaussian bands were consolidated into two individual transitions. The two groups of Gaussian bands are labelled band-1 and -2 (Fig. 1b), which correspond to two individual electronic transitions. Band-1 is composed of G-1, and Band-2 is the sum of Gaussian bands G-2–G-8, where the amplitude of G-8 is too small to be observed in Fig. 1a (Table S1). The maxima of bands 1 and 2 are located at 2.40×10^4, and 2.50×10^4 cm^{-1}, respectively. The G-2 band has the lowest energy among the Gaussian bands composing the band-2, and therefore it can be assigned as the origin (0,0) band of the corresponding transition.

Although the observed vibrational structure in the gas phase was complex, two vibronic bands of energy of 1098 and 1968 cm^{-1} were observed.[17,18] In the PMMA matrix, the Gaussian bands G-4 and G-5 having the vibrational energies of 850 and 1820 cm^{-1} are present (Table S1 in the ESI). It is inferred that G-4 and G-5 correspond to the two vibronic bands identified in the gas phase owing to their similar energies.

The decomposition of the absorption spectra into the two bands provides a reasonable fit of the EA spectra (Fig. 1c), although there are minor inconsistencies at energies above 2.40×10^4 cm^{-1}. Nevertheless, our fitting results are sufficiently reliable for analysing the prominent features of the EA spectra. The coefficients obtained by fitting each EA spectrum were reproduced for the five samples, and the average values of these coefficients are presented in Table 1. Other combinations of the Gaussian bands were attempted to create two absorption bands. For instance, band-1 was presumed to be the sum of the Gaussian bands G-1 – G-7, and band-2 was composed of G-8. However, these combinations resulted in unacceptable fitting results.

Table 1. Fitting coefficients for the EA spectrum of TCNQ.

	A_χ (10^{-2} cm^2 MV^{-2})	B_χ (10 cm MV^{-2})	C_χ (10^4 MV^{-2})
Band-1	0.32	0.23	0.18
Band-2	-0.05	0.04	0.00

The zeroth-, first-, and second-derivative contributions of band-1 and -2 to the fitting of the EA spectra are shown in Fig. 3. The zeroth-derivative components of the two bands make significant and opposing contributions, as shown in Figs. 3a and 3b, respectively. These zeroth-derivative components are attributed to the alterations in the transition dipole moment induced by the applied field, as described by eqns (2) and (7). Furthermore, the amplitudes of the zeroth-derivative components of band-1 and -2 are found to be comparable in terms of absolute magnitude. A similar pairing of the zeroth derivative components of the two absorption bands was reported for the EA spectrum of thioflavin T, which exhibited the mixing of two different excited states. [23]

The zeroth-derivative coefficient A_χ includes the contributions from the transition polarizability ($\boldsymbol{A}$) and transition hyperpolarizability ($\boldsymbol{B}$) (eqns (2 and 7)). According to eqn (2),

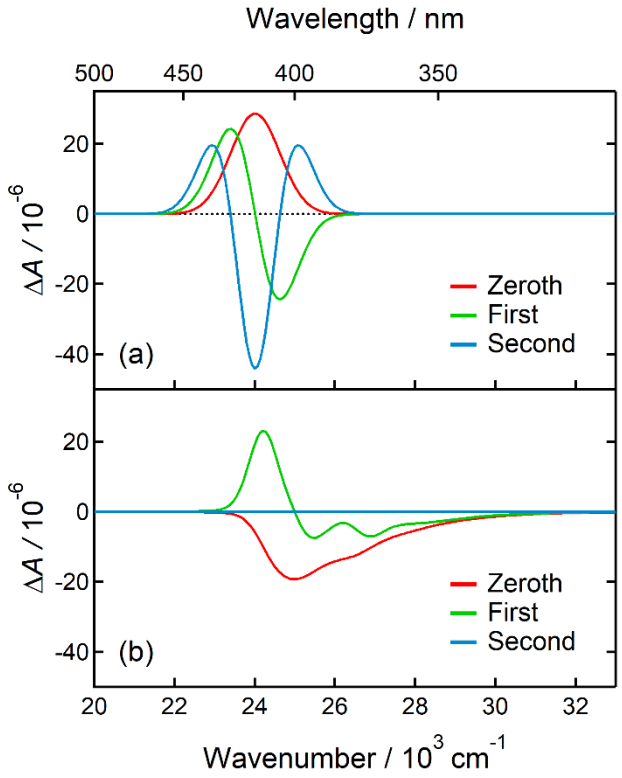

Fig. 3. Contributions of the zeroth- (red line), first- (green line), and second-derivative (blue line) components to the EA spectrum: (a) band-1 and (b) band-2.

the contribution from $\boldsymbol{A}$ is expected to be positive, whereas that from $\boldsymbol{B}$ can be either positive or negative, depending on the magnitude and sign of its components. [34] The negative value of the zeroth-derivative component for band-2, as observed in Fig. 3b, suggests that the contribution from transition hyperpolarizability $\boldsymbol{B}$ dominates the A_χ coefficient, and the contribution of transition polarizability $\boldsymbol{A}$ is comparatively negligible.

The first-derivative coefficient B_χ is composed of contributions from both the polarizability difference $\Delta\bar{\alpha}$ and the change in the transition dipole moment (eqn (3)). Given that the contribution from $\boldsymbol{A}$ is insignificant, the second term in eqn (3) is negligible. Therefore, the coefficient B_χ is attributed to the first term determined by $\Delta\bar{\alpha}$. From the fitting coefficient of the EA spectra (Table 1), $\Delta\bar{\alpha}$ is found to be 85 Å^3 for band-1 (Table 2) whereas band-2 has a smaller $\Delta\bar{\alpha}$ value of 14 Å^3.

A marked contribution from the second-derivative component is observed for band-1 (Fig. 3a). From the observed second-derivative coefficient C_χ (Table 1; eqn (4)), a $\Delta\mu$ value of 6 D is obtained for band-1 (Table 2). By contrast, band-2 shows negligible contribution from the second-derivative component to the EA spectrum (Fig. 3b). In this case, $\Delta\mu \approx 0$ D, demonstrating negligible change in dipole moment upon the excitation of band-2 (Table 2).

Table 2. Parameters and band assignments determined from the EA spectrum fitting of TCNQ.

Parameter	Band-1	Band-2
$\Delta\bar{\alpha}^a$	(8.5 ± 0.9) × 10 Å^3	(1.4 ± 0.4) × 10 Å^3
$\Delta\mu^a$	6 ± 0.2 D	0 D
Assignment	ICT state[b]	LE state[c]

[a]The reported values are not corrected for the internal field factor f_{int}. If we adopt this correction, the values of $\Delta\bar{\alpha}$ and $\Delta\mu$ should be revised to $f_{\text{int}}^{-2}\Delta\bar{\alpha}$ and $f_{\text{int}}^{-1}\Delta\mu$, respectively.
[b]Intramolecular charge-transfer state
[c]Locally excited state

The EA spectrum clearly demonstrated that the absorption band of TCNQ comprised transitions to two excited states with different polarizabilities and dipole moments. The vertical transition energy and oscillator strength (*f*) predicted by CC2 calculations are listed in Table 3. [35] The oscillator strength for the transition to the $^1B_{3u}$ state was predicted to be f = 1.30, indicating that this transition is allowed. f = 0.00 was obtained for the transition to the $^1B_{1g}$ state, suggesting that this transition is forbidden. TD-DFT calculations of the excited states of TCNQ at the M06-2X/6-311++G(d,p) level have been performed by Muramatsu et al. [17, 18, 35] By minimizing the energies of the excited states, the energy gap between the $^1B_{3u}$ and $^1B_{1g}$ states became only approximately 720 cm^{-1} at the adiabatic energy level of the $^1B_{1g}$ state. The electron density difference between the $^1B_{1g}$ and ground states was calculated using the Kohn–Sham orbitals of the DFT calculations, which showed that the electron was transferred from the phenyl ring to the four CN groups upon the transition. Therefore, the $^1B_{1g}$ state was characterized by ICT. The EA spectra acquired in this study provide for the first time experimental evidence for the ICT characteristics of the nonemissive state.

The transition to the $^1B_{1g}$ state should be forbidden (f = 0) according to the molecular symmetry of the D_{2h} point group, and a consistent result was obtained from the calculations (Table 3). In the absorption spectrum (Fig. 1b), band-1 has a comparatively minor contribution and weaker intensity than that of band-2, which undergoes negligible change in the dipole moment (0 D). The dipole moment changes upon the transition to band-1 (6 D). Based on these results, band-1, with its weaker intensity, was assigned to the $^1B_{1g}$ state with ICT characteristics, and band-2 was assigned to the transition to the $^1B_{3u}$ state.

Table 3. Vertical transition energy (*E*) and oscillator strength calculated at CC2/aug-cc-pVTZ level.[a]

Excited states (symmetry)	*E* / eV	*f*
S_1 ($^1B_{3u}$)	3.29	1.30
S_2 ($^1B_{1g}$)	3.81	0.00

[a]Reproduced from ref. 35.

The dependence of the fluorescence properties of TCNQ on the solvent polarity was explained by assuming the existence of two excited states.[15-17] In a previous transient absorption (TA) study, a relaxation mechanism between the nonemissive and emissive states was proposed to explain the excited-state dynamics.[13] However, these studies could not conclude that the nonemissive state was ascribed to the ICT state. The EA measurements in this study clearly reveal the existence of the nonemissive state with ICT character and the emissive state, which corresponds to the LE state. The nonemissive ICT state assumed in the fluorescence and transient absorption spectroscopies can be assigned to the $^1B_{1g}$ state. This assignment is in agreement with that suggested by Muramatsu et al. [18] The $^1B_{3u}$ state of band-2 shows f = 1.30 (Table 3). The emissive LE state assumed in the previous spectroscopic studies can be assigned to the $^1B_{3u}$ state.

The energy levels listed in Table 3 are calculated for the gas phase, where the energy level of the $^1B_{3u}$ state (band-2) is slightly lower than that of the $^1B_{1g}$ state (band-1). There could be two possible explanations for the difference in the order of the energy levels of the experimentally determined and calculated excited states. First, there could be errors in the calculation of the excited-state energy levels. Second, the energy shift of the electronic transition could be caused by solute–solvent interactions in the polymer matrix, which should increase with an increase in the dipole moment and polarizability of the solute molecules. [36] The $^1B_{1g}$ state has the characteristics of an ICT state with a larger dipole moment and polarizability as compared to those of the $^1B_{3u}$ state (Table 2). Therefore, the energy shift caused by the solute–solvent

interactions should be larger for the $^1B_{1g}$ state of band-1. This difference in the energy shift could result in the experimentally observed order of the excited states.

The presence of zeroth-derivative components for both the LE state (band-2) and ICT state (band-1) in the EA spectrum suggests that the transition dipole moments of these states are altered by the electric field. In the EA spectrum, the zeroth-derivative component of the ICT state contributes positively, whereas that of the LE state contributes negatively (Fig. 3). This result indicates the mixing between the LE and ICT states, which is enhanced by the perturbation of the electric fields. The oscillator strength of the LE state is transferred to that of the ICT state in the presence of electric fields. The matrix element that describes the state mixing by static electric fields is represented as $\langle \Psi(^1B_{3u}) | \widehat{H_F} | \Psi(^1B_{1g}) \rangle$, where $\Psi(^1B_{3u})$ and $\Psi(^1B_{1g})$ denote the electronic wave functions of the LE and ICT states, respectively, and $\widehat{H_F}$ is the electric-field perturbation operator. The matrix element is necessarily zero unless the direct product of the symmetry species of the wave functions and the operator contains a totally symmetric irreducible representation. An electric field of strength *F* in the *y*-direction corresponds to the perturbation operator $\widehat{H_F} = -\mu_y F$, where μ_y is the *y*-component of the electric dipole operator (Fig. 4). The perturbation operator of the electric field in the *y*-direction contains a symmetrical species B_{2u} of odd parity; thus, the electric field mixes the electronic states of opposite parity. It follows that the direct product in the matrix element contains A_g if the electric field has a *y*-component. Therefore, the $^1B_{3u}$ (LE) state was mixed with the $^1B_{1g}$ (ICT) state when the molecule was perturbed by applying an electric field in the *y*-direction. The observation of the zeroth-derivative component in the EA spectrum and state mixing in the presence of *F* are corroborated by the symmetry arguments of the electronic states.

In previous studies, deactivation from the LE state to the ICT state was assumed to be the mechanism responsible for the characteristic fluorescence properties of TCNQ, such as an unusually long fluorescence lifetime and an acute response to solvent polarity. [16, 17] The EA spectra acquired in this study clearly demonstrate mixing between the emissive LE and nonemissive ICT states. The mixing rationalizes the efficient relaxation from the LE state to the ICT state.

The structure of the ground state of TCNQ belongs to the D_{2h} point group. The symmetry species in the ICT state was assigned as $^1B_{1g}$ in the D_{2h} group. The EA spectrum showed that the permanent dipole moment of the molecule changed by 6 D upon transition to the ICT state (Table 2). Since the permanent dipole moment of the ground state (^1A_g) must be zero, the ICT state should have a dipole moment of 6 D. The molecules belonging to group D_{2h} have parity symmetry owing to the centre of inversion. Symmetry arguments indicate that the permanent dipole moment of TCNQ, even in the excited states, must be zero unless the symmetry of the D_{2h} group is broken. Therefore, the EA spectrum demonstrates that symmetry is broken in the ICT state in the PMMA matrix. It follows that the symmetry of the minimum-energy structure on the potential energy surface of the ICT state deviates from D_{2h}.

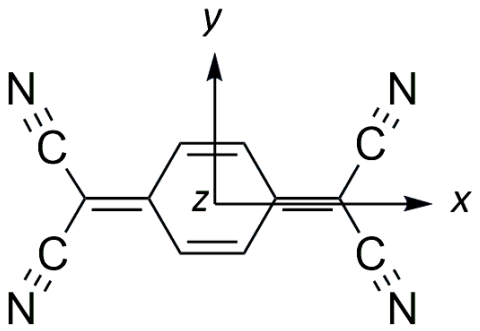

Fig. 4. Chemical structure of TCNQ and the molecule-fixed axes.

The optimized structures in the ground and excited states in the gas phase were calculated using the (TD-)DFT and CC2 methods.[17,18,35] The optimized structures in the ground and $^1B_{3u}$ states belong to the D_{2h} point group. A zero electric dipole moment is imposed on molecules with D_{2h} symmetry because of the inversion symmetry. The molecule vertically excited to the $^1B_{1g}$ state was calculated to be optimized to a slightly deformed structure belonging to the C_{2h} group.[18] However, this structure also has the inversion symmetry, resulting in a zero dipole moment. The observed dipole moment change ($\Delta\mu$ = 6 D) upon the transition to the ICT state can be ascribed to the symmetry breaking to lower symmetry than C_{2h}, which would be induced by the solvent effects in the excited state.

Conclusions

EA spectroscopy was used to study the Stark effect on the absorption spectrum of TCNQ dispersed in the PMMA matrix. The analysis of the Stark effect revealed that the two absorption bands having different $\Delta\mu$ and $\Delta\bar{\alpha}$ values overlapped in the absorption band and thus seemingly appeared as a single electronic state. The two absorption bands were assigned to the ICT and LE states. The change in dipole moment was 6 D / f_{int} for the ICT state and 0 D for the LE state. Mixing between the ICT and LE states was augmented in the presence of an external electric field. This admixture was consistently explained by symmetry arguments. Symmetry breaking in the ICT state was predicted because a significant permanent dipole moment emerged upon the transition from the ground state to the ICT state. These results provide direct experimental evidence for the existence of a nonemissive ICT state in the excited state of TCNQ, substantiating the hypotheses proposed in previous studies. Our results contribute to an in-depth understanding of the photophysics of TCNQ, a valuable electron-acceptor molecule that has been extensively utilized in chemical and physical studies.

Author Contributions

Conceptualization, Supervision, Funding acquisition, Project administration, Methodology: T. I. ; Writing – original draft, Investigation, Visualization: A. I., K. S. ; Formal analysis: T. I., A. I., K. S. ; Validation, Writing – review, and editing: T. I. and A. I.

Conflicts of interest

There are no conflicts to declare.

Acknowledgements

T.I. acknowledges the financial support from the Muroran Institute of Technology, KAKENHI [No. JP16K05950] from JSPS, and the CASIO Science Promotion Foundation.

References

1 J. S. Brooks, *Chem. Soc. Rev.*, 2010, **39**, 2667-2694.
2 T. Akutagawa, *Bull. Chem. Soc. Jpn.*, 2021, **94**, 1400-1420.
3 M. Takeda, K. Umemoto, T. Nohara, K. Tozawa, J. Matsui and A. Masuhara, *J. Electrochem. Soc.*, 2019, **166**, B3131.
4 H. He, K. H. Kim, A. Danilov, D. Montemurro, L. Y. Yu, Y. W. Park, F. Lombardi, T. Bauch, K. Moth-Poulsen, T. Lakimov, R. Yakimova, P. Malmberg, C. Muller, S. Kubatkin and S. Lara-Avila, *Nature Commun.*, 2018, **9**.
5 M. Abdelfatah, O. H. Basyouni, W. Ismail and A. El-Shaer, *J. Alloys Compd.*, 2023, **936**, 168329.
6 I. Salzmann, G. Heimel, M. Oehzelt, S. Winkler and N. Koch, *Acc. Chem. Res.*, 2016, **49**, 370-378.
7 H. Miyasaka, *Bull. Chem. Soc. Jpn.*, 2021, **94**, 2929-2955.
8 Y. Zhao, A. Opitz, A. Eljarrat, Z. Kochovski, C. T. Koch, N. Koch and Y. Lu, *ACS Appl. Nano Mater.*, 2021, **4**, 11625-11635.
9 H. Alves, R. M. Pinto and E. S. Maçôas, *Nature Commun.*, 2013, **4**, 1842.
10 A. Rubino, A. Camellini and I. Kriegel, *Opt. Mater. X*, 2021, **11**, 100081.
11 H. T. Jonkman, G. A. van der Velde and W. C. Nieuwpoort, *Chem. Phys. Lett.*, 1974, **25**, 62-65.
12 R. Girlanda, G. Martino, A. M. Mezzasalma, G. Mondio and G. Saitta, *Il Nuovo Cimento D*, 1986, **8**, 229-241.
13 T. Iimori, Y. Torii, T. Ishikawa and N. Tamai, *J. Phys. Chem. B*, 2020, **124**, 7918-7928.
14 T. Iimori, T. Ishikawa, Y. Torii, H. Tamaya, H. Nakano and M. Kanno, *Chem. Phys. Lett.*, 2020, **738**, 136912.
15 H. Tamaya, Y. Torii, T. Ishikawa, H. Nakano and T. Iimori, *ChemPhysChem*, 2019, **20**, 2531-2538.
16 H. Tamaya, H. Nakano and T. Iimori, *J. Lumin.*, 2017, **192**, 203-207.
17 N. Chaki, S. Muramatsu, Y. Iida, S. Kenjo, Y. Inokuchi, T. Iimori and T. Ebata, *ChemPhysChem*, 2019, **20**, 996-1000.
18 S. Muramatsu, N. Chaki, S.-n. Kinoshita, Y. Inokuchi, M. Abe, T. Iimori and T. Ebata, *RSC Adv.*, 2021, **11**, 22381-22389.
19 L. Ma, P. Hu, C. Kloc, H. Sun, M. E. Michel-Beyerle and G. G. Gurzadyan, *Chem. Phys. Lett.*, 2014, **609**, 11-14.
20 S. G. Boxer, *J. Phys. Chem. B*, 2009, **113**, 2972-2983.
21 D. de Sa Pereira, C. Menelaou, A. Danos, C. Marian and A. P. Monkman, *J. Phys. Chem. Lett.*, 2019, **10**, 3205-3211.
22 T. Iimori, R. Ito and N. Ohta, *J. Phys. Chem. A*, 2016, **120**, 5497-5503.
23 A. Islam, Y. Kikuchi and T. Iimori, *J. Phys. Chem. A*, 2023, **127**, 1436-1444.
24 T. Iimori, R. Ito, N. Ohta and H. Nakano, *J. Phys. Chem. A*, 2016, **120**, 4307-4313.
25 G. U. Bublitz and S. G. Boxer, *Ann. Rev. Phys. Chem.*, 1997, **48**, 213-242.
26 C. M. Legaspi, R. E. Stubbs, M. Wahadoszaman, D. J. Yaron, L. A. Peteanu, A. Kemboi, E. Fossum, Y. Lu, Q. Zheng and L. J. Rothberg, *J. Phys. Chem. C*, 2018, **122**, 11961-11972.
27 D. M. D'Alessandro, P. H. Dinolfo, M. S. Davies, J. T. Hupp and F. R. Keene, *Inorg. Chem.*, 2006, **45**, 3261-3274.
28 N. Ohta, *Bull. Chem. Soc. Jpn.*, 2002, **75**, 1637-1655.
29 W. Liptay, in *Excited States*, ed. E. C. Lim, Elsevier, 1974, vol. 1, pp. 129-229.
30 Y.-g. K. Shin, B. S. Brunschwig, C. Creutz and N. Sutin, *J. Phys. Chem.*, 1996, **100**, 8157-8169.
31 L. L. Premvardhan and L. A. Peteanu, *J. Phys. Chem. A*, 1999, **103**, 7506-7514.
32 G. Beadie, M. Brindza, R. A. Flynn, A. Rosenberg and J. S. Shirk, *Appl. Opt.*, 2015, **54**, F139-F143.
33 R. Ito, Y. Funamoto, N. Ohta and T. Iimori, *Chem. Phys.*, 2015, **456**, 1-7.
34 G. U. Bublitz, R. Ortiz, S. R. Marder and S. G. Boxer, *J. Am. Chem. Soc.*, 1997, **119**, 3365-3376.
35 T. Iimori, *Comput. Theor. Chem.* 2021, **1199**, 113211.
36 Valeur and M. N. Berberan-Santos, *Molecular Fluorescence: Principles and Applications, Second Edition*, Wiley-VCH Verlag GmbH & Co. KGaA, Weinheim, Germany, 2013.